# Electrohydrodynamics of drops and vesicles

**Petia M. Vlahovska**

Department of Engineering Sciences and Applied Mathematics, Northwestern University, Evanston, USA, 60208

Xxxx. Xxx. Xxx. Xxx. YYYY. AA:1–27

https://doi.org/10.1146/((please add article doi))



**Keywords**

electrohydrodynamics, Stokes flow, instability, streaming, electrorotation, Quincke, electrorheology, electroporation

**Abstract**

The 1969 review by J. R. Melcher and G. I. Taylor defined the field of electrohydrodynamics. Fifty years on, the interaction of weakly conducting (leaky dielectric) fluids with electric fields continues to yield intriguing phenomena. The prototypical system of a drop in an uniform electric field has revealed remarkable dynamics in strong electric fields such as symmetry–breaking instabilities (e.g., f rotation), and streaming from the drop equator. This review summarizes recent experimental and theoretical studies in the area of fluid particles (drop and vesicles) in electric fields, with focus on the transient dynamics and extreme deformations. A theoretical framework to treat the time evolution of nearly-spherical shapes is provided. The model has been successful in describing the dynamics of vesicles (closed lipid membranes) in electric field, highlighting the broader range of applicability of the leaky dielectric approach.

## 1. INTRODUCTION

The electric field induced fluid flows around a droplet (Melcher & Taylor 1969) excited long-standing interest in the field of electrohydrodynamics. In his pioneering paper, G. I. Taylor formulated the leaky dielectric model (LDM) and predicted the steady drop shape in the small-deformation limit (Taylor 1966). Subsequent body of work, reviewed in (Lac & Homsy 2007, Saville 1997), experimentally tested the validity of the model, derived more accurate analytical solutions, and developed numerical simulations to explore large drop deformations, stability and break-up. This review focuses on the latest developments in understanding electrohydrodynamics, in particular, the unsteady dynamics of drops and vesicles (non-spherical capsules made of lipid bilayer membranes). Electrosprays are not discussed here as the topic merits a separate review (de la Mora 2007, Ganan-Calvo et al. 2018).

## 2. THE LEAKY DIELECTRIC MODEL

Electrohydrodynamic flows are driven by electric stresses shearing fluid interfaces. The tangential electric stresses are due to the electric field acting on free charges accumulated at boundaries separating media (fluids) with different permittivities and conductivities. Here, we formulate the LDM for a drop in an electric field, the prototypical electrohydrodynamic problem (Taylor 1966). In Section 3 we summarize the analytical solution for small drop deformations, and numerical and experimental results for drop behavior in strong fields. In Section 4 we extend the LDM to vesicles, which are biomimetic capsules made of a lipid bilayer membrane. The details of the small deformation theories of drops and vesicles are available in the supplemental Mathematica file.

### 2.1. Governing equations

Consider a neutrally buoyant drop with radius $a$ and no net charge. The drop and the continuous phase are Newtonian fluids, with viscosities $\hat{\eta}$ and $\eta$, permittivities $\hat{\varepsilon}$ and $\varepsilon$, and conductivities $\hat{\sigma}$ and $\sigma$, respectively ( $\hat{}$ denotes quantity associated with the drop fluid). The interfacial tension $\gamma$ is only affected by surfactants. The mismatch in fluids properties is characterized by the three ratios

$$R = \frac{\hat{\sigma}}{\sigma}\,, \quad S = \frac{\hat{\varepsilon}}{\varepsilon}\,, \quad \lambda = \frac{\hat{\eta}}{\eta}\,. \tag{1.}$$

The drop is placed in a uniform electric field with magnitude $E_0$,

$$\mathbf{E}^{\infty} = E_0 \hat{\mathbf{z}}\,. \tag{2.}$$

The LDM assumes irrotational electric field (hence $\mathbf{E} = -\nabla\Phi$, where $\Phi$ is the electric potential), electroneutral bulk fluids and that the electric current obeys Ohm's law

$$\nabla\cdot(\sigma\mathbf{E}) = 0\,, \qquad \nabla\cdot\left(\hat{\sigma}\hat{\mathbf{E}}\right) = 0\,. \tag{3.}$$

Fluid motion is described by the Stokes equations, since the Reynolds number for the fluids and small drops typically studied are small. The velocity, $\mathbf{u}$, and dynamic pressure, $p$, satisfy

$$\eta\nabla^2\mathbf{u} = \nabla p\,, \qquad \nabla\cdot\mathbf{u} = 0\,, \quad \hat{\eta}\nabla^2\hat{\mathbf{u}} = \nabla\hat{p}\,, \qquad \nabla\cdot\hat{\mathbf{u}} = 0\,. \tag{4.}$$

The assumption of charge-free fluids decouples the electric and hydrodynamic fields in the bulk. The coupling occurs at the drop interface, through the boundary conditions for ($a$) mechanical equilibrium, and ($b$) conservation of surface charge.

The hydrodynamic and electric tractions at the interface are discontinuous and balanced by interfacial stresses $\mathbf{t}_s$

$$\mathbf{n}\cdot\left[\left(\mathbf{T}-\hat{\mathbf{T}}\right)+\left(\mathbf{T}^{\mathrm{el}}-\hat{\mathbf{T}}^{\mathrm{el}}\right)\right]=\mathbf{t}_s\,, \tag{5.}$$

where $\mathbf{n}$ is the outward pointing normal vector. $T_{ij}=-p\delta_{ij}+\eta(\partial_j u_i+\partial_i u_j)$ is the hydrodynamic stress and $\delta_{ij}$ is the Kronecker delta function. The electric stress is given by the Maxwell stress tensor $T^{\mathrm{el}}_{ij}=\varepsilon\left(E_iE_j-E_kE_k\delta_{ij}/2\right)$. In the case of a drop, $\mathbf{t}_s=\gamma\,\mathbf{n}\,(\nabla\cdot\mathbf{n})$ is the capillary stress due to curvature along the deformed drop interface (assuming constant interfacial tension, i.e., surfactant-free interface). The interfacial stresses can be more complex due to interfacial viscosity, Marangoni stresses (when surfactants are present), or shear and bending elasticity (in case of capsules and bilayer vesicles).

Charge conservation at the drop surface requires that

$$\sigma\mathbf{n}\cdot\left(\mathbf{E}-R\hat{\mathbf{E}}+R_s\nabla_s\cdot\mathbf{E}\right)=-\frac{\partial Q}{\partial t}-\nabla_s\cdot(\mathbf{u}Q)\,, \tag{6.}$$

where $R_s=\sigma_s/\sigma a$ is the surface conductivity. The formulation is completed by assuming continuity of the electric potential and velocity across the drop surface: $\Phi=\hat{\Phi}$ and $\mathbf{u}=\hat{\mathbf{u}}$. If charge convection is neglected, then for a given drop shape the electrostatic system yields the electric field and electric stresses. For a spherical drop the electric field is given in the sidebar titled *A sphere in a uniform electric field*. Once the electric stresses are known, the fluid flow and drop shape are determined from the stress balance Eq. 5. Accounting for the charge convection is challenging as it requires that the electrostatic and flow problems are solved simultaneously. Finally, the induced charge $Q$ is determined from the jump in the displacement field

$$Q=\varepsilon\mathbf{n}\cdot\left(\mathbf{E}-S\hat{\mathbf{E}}\right)\,. \tag{7.}$$

## 2.2. Characteristic time-scales and dimensionless parameters

In describing the shape evolution, all variables are nondimensionalized using the radius of the undeformed drop $a$, the field strength $E_0$, a characteristic applied stress $\tau_c=\varepsilon E_0^2$, and the properties of the suspending fluid. Accordingly, the time scale for the electrohydrodynamic flow is $t_c=\eta/\tau_c$ and the velocity scale is $u_c=a\tau_c/\eta$. The conduction process in the suspending fluid occurs on time scale given by the charge relaxation time $t_e=\varepsilon/\sigma$. The charge relaxation time in the drop is $\hat{t}_e=\hat{\varepsilon}/\hat{\sigma}$. Drop relaxation towards equilibrium spherical shape occurs on the surface tension time scale $t_\gamma=\eta a/\gamma$. These four time scales form the three nondimensional parameters that are most commonly used to quantify electrohydrodynamic flows

$$\frac{R}{S}=\frac{t_e}{\hat{t}_e}\,,\quad Ca=\frac{t_\gamma}{t_c}=\frac{\varepsilon E_0^2 a}{\gamma}\,,\quad Re_E=\frac{t_e}{t_c}=\frac{\varepsilon^2E_0^2}{\sigma\eta}\,. \tag{8.}$$

$Ca$ and $Re_E$ are the capillary and electric Reynolds numbers.

It is instructive to estimate the magnitude of the characteristic time scales involved in the electrohydrodynamics of leaky dielectric drops in strong fields. Typical experimental

## A SPHERE IN A UNIFORM ELECTRIC FIELD

Here we summarize the electrostatics of a spherical drop when charge convection is negligible. In a spherical coordinate system centered at the drop, the electric potential is

$$\Phi = aE_0 Re\left\{\Psi e^{\mathrm{i}\omega t}\right\}\cos\theta\,, \quad \text{where} \quad \Psi = -(r + Pr^{-2})\,, \quad \hat{\Psi} = -P_{\mathrm{p}} r\,,$$

where $\theta$ is the angle with the applied field.

In a uniform AC field, $\mathbf{E} = E_0\cos(\omega t)\hat{\mathbf{z}}$,

$$P(\omega) \equiv P^{AC}(\omega) = P_{\mathrm{p}}(\omega) - 1 = \frac{k_{\mathrm{s}} - k_{\mathrm{p}} - 2R_s}{2k_{\mathrm{s}} + k_{\mathrm{p}} + 2R_s}\,, \quad k_{\mathrm{p}} = R + \mathrm{i}\omega S\,, \quad k_{\mathrm{s}} = 1 + \mathrm{i}\omega\,.$$

Upon application of a uniform DC field, $\mathbf{E} = E_0\hat{\mathbf{z}}$, the free charge at the drop surface builds up on a time scale given by the Maxwell-Wagner polarization time $t_{\mathrm{mw}}$,

$$P(t) = P_{\mathrm{p}}(t) - 1 = P^{AC}(\omega = 0)\left(1 - e^{-t/t_{\mathrm{mw}}}\right)\,, \qquad t_{\mathrm{mw}} = \frac{\varepsilon}{\sigma}\frac{S+2}{R+2R_s+2}\,.$$

### Induced dipole

The effective dipole $\mathbf{P}$ due to the induced free surface charge $Q$ is

$$\begin{aligned}\mathbf{P} =& 4\pi\varepsilon a^3\left[P^{AC}(0) - P^{AC}(\infty)\right]\left(1 - e^{-t/t_{\mathrm{mw}}}\right)\mathbf{E}\,,\\ Q =& \varepsilon E_0\left[P^{AC}(0) - P^{AC}(\infty)\right]\left(1 - e^{-t/t_{\mathrm{mw}}}\right)\cos\theta\,,\end{aligned}$$

where $P^{AC}(0)$ and $P^{AC}(\infty)$ are the low- and high-frequency drop fluid susceptibilities

$$P^{AC}(0) - P^{AC}(\infty) = 3\frac{R + 2R_s - S}{R + 2R_s + 2}\,.$$

conditions involve electric fields of the order of $E_0 \sim$1kV/cm and fluids with conductivities in the range $\sigma \sim 10^{-10} - 10^{-12}$ S/m, viscosity $\eta \sim 1$ Pa.s, and $\gamma \sim 10^{-3}$ N/m. Hence, the flow, capillary and charge time scales can be comparable, $\sim 0.1 - 10$ s. The interplay between these time scales gives rise to a rich phenomenology of drop dynamics in strong electric field.

## 3. DROPS

LDM predicts that in weak uniform electric fields a drop adopts a spheroidal shape axisymmetrically aligned with the applied field. As the field strength increases, the drop undergoes various types of instabilities.

### 3.1. Transient deformation in weak fields, $Ca \ll 1$

Drop shape remains nearly spherical if $Ca \ll 1$. Analytical solutions for drop electrodeformation in this regime and for negligible charge convection have been developed by Esmaeeli & Sharifi (2011), Lanauze et al. (2013). If fluid inertia and polarization relaxation are neglected, this theory predicts a monotonic approach to the steady shape. If polarization relaxation occurs on a time scale comparable to the shape evolution ($t_{\rm mw} \sim t_c$), in the case $R/S < 1$, a transient prolate shape can form before the ultimate oblate shape (Lanauze et al. 2013, 2015). The effect of charge convection on transient drop deformation has been analyzed by (Das & Saintillan 2017b). The main results from the linear deformation theory are summarized in the sidebar *Drop deformation in a uniform electric field.*

Drop deformation in nonuniform field (e.g., axisymmetric quadrupolar field) has been analyzed by (Deshmukh & Thaokar 2013) assuming instantaneous polarization and no charge convection, i.e., steady current balance Eq. 6.

In this Section we provide the leading-order small-$Ca$ evolution equations for arbitrary drop shape (ellipsoidal, quadrupolar etc.). Interfacial viscosity is included in the model. For small deviations from sphericity, the instantaneous shape is described as the radial position of the interface $r_s = a(1 + f(t, \theta, \varphi))$. It is convenient to expand all variables in spherical harmonics $f = \sum f_{jm}(t) Y_{jm}(\theta, \varphi)$, where $Y_{jm} = (-1)^m P_j^m(\cos\theta)\, e^{{\rm i}m\varphi}$. A uniform electric field is described by $j = 1$ spherical harmonic and directly excites $j = 2$ deformation.

The shape evolves in a general electric field as (Vlahovska 2016):

$$\frac{\partial f_{jm}}{\partial t} = \frac{\alpha_{j0}\left(\tau^{\rm el}_{jm0} + \tau^{s}_{jm0}\right) + \alpha_{j2}\left(\tau^{\rm el}_{jm2} + \tau^{s}_{jm2}\right)}{c_2\lambda^2 + c_1\lambda + c_0}\,, \tag{9.}$$

where

$$\alpha_{j0} = j(j+1)\left(2(j+1)j\lambda^{\rm mm}_{\kappa} + 3(j+1)\lambda + 3j\right) \tag{10.}$$

$$\alpha_{j2} = j(j+1)\left(\left(j^2+j-2\right)\lambda^{\rm mm}_{\eta} + (j+1)j\lambda^{\rm mm}_{\kappa} + (2j+1)\lambda + 2j + 1\right) \tag{11.}$$

$$\begin{aligned} c_2 =& 2\left(2j^4 + 4j^3 + j^2 - 4j - 3\right) \\ c_1 =& 8j^4 + 16j^3 + 4j^2 - 4j + 3 + \left(2j^4 + 5j^3 + 3j^2 - 5j - 5\right) j\lambda^{\rm mm}_{\kappa} \\ &+ \left(2j^5 + 5j^4 + 3j^3 + j^2 - 5j - 6\right)\lambda^{\rm mm}_{\eta} \\ c_0 =& j(j+2)\left[\left(4j^2+2\right) + \lambda^{\rm mm}_{\kappa}\left(4\left(j^2-1\right)\lambda^{\rm mm}_{\eta} + \left(2j^3 + j^2 + j + 2\right)\right)\right. \\ &\left. + \lambda^{\rm mm}_{\eta}\left(2j^3 + j^2 + j - 4\right)\right] \quad NOTE: TYPO! \end{aligned} \tag{12a.}$$

$\lambda^{\rm mm}_{\kappa} = \eta^{\kappa}/a\eta$ and $\lambda^{\rm mm}_{\eta} = \eta^{s}/a\eta$ are the dimensionless surface dilatational and shear viscosities. The interfacial stresses on the drop are

$$\tau^{s}_{jm0} = 0\,, \quad \tau^{s}_{jm2} = -\,Ca^{-1}\left(-2 + j(j+1)\right) f_{jm}\,. \tag{13.}$$

The electric stresses for a DC field that is a combination of uniform and linear field $\mathbf{E} = e_u\nabla(rY_{10}) + e_q\nabla(r^2Y_{20})$ are listed below. $e_q = 0$ and $e_u = 1$ specifies a uniform electric field along the z direction, and $e_u = 0$ and $e_q = \epsilon$ ($\epsilon$ being the dimensionless field gradient) defines an axisymmetric (around the z axis) quadrupole electric field $\epsilon(-x, -y, 2z)$.

$$\begin{aligned} \tau^{\rm el}_{200} &= e_u^2\frac{3\,(R-S)}{(R+2)^2} + e_q^2\frac{50}{7}\frac{R-S}{(2R+3)^2}\,, \quad \tau^{\rm el}_{400} = e_q^2\frac{90}{7}\frac{R-S}{2R+3}\,, \\ \tau^{\rm el}_{202} &= e_u^2 3\frac{1+R^2-2S}{(R+2)^2} - e_q^2\frac{25}{7}\frac{3-4R^2+S}{(2R+3)^2}\,, \quad \tau^{\rm el}_{402} = e_q^2\frac{180}{7}\frac{1+R^2-2S}{(R+2)^2} \end{aligned} \tag{14.}$$

## DROP DEFORMATION IN A UNIFORM DC ELECTRIC FIELD, $Ca \ll 1$

### Shape evolution:

The shape of the drop is an axisymmetric ellipsoid parametrized by $r_s = a(1 + s(t)P_2(\cos\theta))$. Drop deformation is usually characterized by the Taylor deformation parameter $D = (a_{||} - a_\perp)/(a_{||} + a_\perp)$, where $a_{||}$ and $a_\perp$ are the drop axes parallel and perpendicular to the applied field direction; $D = 3s/4$. Upon application of an uniform electric field, shape evolution is described by

$$\frac{\partial s}{\partial t} = \frac{40(1+\lambda)}{(3+2\lambda)(16+19\lambda)}\left[\frac{3}{4}F(R,S,\lambda,t) - Ca^{-1}\, s(t)\right],$$

where

$$F(R,S,\lambda,t) = \frac{(16+19\lambda)}{45(1+\lambda)}\left(1 - S - (1+2S)\,P(t\delta_{\rm mw}) + \left(\frac{13+7\lambda}{(16+19\lambda)} - S\right)P^2(t\delta_{\rm mw})\right)$$

where

$$P(\tau) = \frac{(1-R)}{(2+R)}\left(1 - e^{-\tau}\right).$$

$\delta_{\rm mw} = t_c/t_{\rm mw}$ is the ratio of the electrohydrodynamic and polarization time scales. If polarization relaxation is instantaneous ($t_{\rm mw} \ll t_c$, i.e., $\delta_{\rm mw} \gg 1$), then the steady shape is monotonically approached

$$D(t) = D_T\left(1 - e^{-t/t_r}\right) \quad \text{where} \quad t_r = \frac{\eta a}{\gamma}\left(\frac{(3+2\lambda)(16+19\lambda)}{40(1+\lambda)}\right)$$

and

$$D_T = \frac{9Ca}{16}F^T(R,S,\lambda), \quad F^T = \frac{1}{(2+R)^2}\left[R^2 + 1 - 2S + 3(R-S)\frac{2+3\lambda}{5(1+\lambda)}\right].$$

If the dipole evolves on a time scale comparable to the flow time scale ($t_{\rm mw} \sim t_c$) the approach to steady state may be nonmonotonic.

### Interfacial velocity

At steady state, the fluid undergoes axisymmetric flow about the drop. The velocity at the drop surface $r = a$ is

$$\mathbf{u}_T = \frac{a\varepsilon E_0^2}{\eta}\frac{9(S-R)}{10(1+\lambda)S(R+2)^2}\sin(2\theta)\hat{\boldsymbol{\theta}},$$

### Classification of drop shape and electrohydrodynamic flow configurations:

The Taylor discrimination function, $F^T$, and the direction of the interfacial flow defined three cases:
**Prolate A**: ($F^T > 0$, $R/S > 1$) flow is from the equator to the pole, drop elongates along the field direction
**Prolate B**: ($F^T > 0$, $R/S < 1$) flow is from the pole to the equator, drop elongates along the field direction
**Oblate**: ($F^T < 0$, $R/S < 1$) flow is from the pole to the equator, drop compresses along the field direction

$$\tau^{\rm el}_{300} = 4\tau^{\rm el}_{300} = e_u e_q \frac{12\,(R-S)}{(R+2)(2R+3)}\,,$$
$$\tau^{\rm el}_{102} = -e_u e_q \frac{6\,\big(3-4R^2+S\big)}{(R+2)(2R+3)}\,, \quad \tau^{\rm el}_{302} = e_u e_q \frac{18\,\big(1+R^2-2S\big)}{(R+2)(2R+3)} \tag{15.}$$

Eq. 9-Eq. 15 provide a unified description of drop deformation in combined uniform and linear fields, and enable compact derivation of some published results. The equations can be further applied to study analytically unexplored problems such as the transient drop deformation in linear fields.

For example, the monotonic evolution towards steady drop shape reported by Esmaeeli & Sharifi (2011) and listed in the sidebar titled Drop Deformationin a Uniform Direct Current Electric Field ($Ca \ll 1$) is obtained from these equations with $e_q = 0$. The results of Deshmukh & Thaokar (2013) for a drop axisymmetrically centered in a quadrupolar field are obtained by setting $e_u = 0$ . If the drop is off-center, i.e., $e_u \neq 0$ and $e_q \neq 0$, it undergoes dielectrophoresis (translation towards or away from the field minimum). If the drop is displaced along the axis of symmetry ($z$) of the quadrupolar field component, the drop translational velocity is $V_z = \partial f_{10}/\partial t$. Thus, from Eq. 9 one can obtain the dielectrophoretic velocity of a spherical drop in a straightforward manner, including the surface viscosity (Mandal & Chakraborty 2017b)

$$\begin{aligned} V_{dep} =& 2e_u e_q \frac{2\lambda\,(R-1)\,(3+2R)+4R^2+R-6}{(2+3\lambda)(2+R)(3+2R)} \\ &+ 4e_u e_q \lambda^{\rm mm}_\kappa \frac{6+R-4R^2-3S}{3(2+2\lambda^{\rm mm}_\kappa+3\lambda)(2+R)(3+2R)} \end{aligned} \tag{16.}$$

The limit of high surface viscosity recovers the result for a rigid sphere $V_{dep} = e_u e_q \frac{4}{3}(R-1)/(2+R)$; in the absence of surface viscosity, Eq. 16 reduces to the clean drop expression derived by (Feng 1996).

## 3.2. Electroheology

Electric fields are often used to control the flow and structure of colloidal suspensions (Bharti & Velev 2015, Dobnikar et al. 2013, Sheng & Wen 2012, van Blaaderen et al. 2013). Of particular interest is how fluid properties such as viscosity are affected by an electric field. For example, application of an electric field perpendicular to the shear flow can enhance the fluid viscosity thousands-fold (this is the so called positive electrorheological effect, PER) (Larson 1999). However, negative electrorheological effect (NER), i.e., viscosity decrease with increasing electric field strength, has also been reported (Huang et al. 2011, Lemaire et al. 2008).

Theoretically, the effective stress $\mathbf{T}_{eff}$ of a sheared dilute suspension, in which hydrodynamic interactions between the particles are negligible, is found from the individual particle stresslet $\mathbf{S}$ (Kim & Karrila 1991)

$$\mathbf{T}_{eff} = \eta\dot{\gamma}\,(2\mathbf{\Gamma}^s + \phi\mathbf{S})\,, \tag{17.}$$

where $\phi$ is the particle volume fraction, $\mathbf{\Gamma}^s$ is the symmetric part of the gradient velocity tensor describing the extensional component of the shear flow, $\mathbf{\Gamma}^s \cdot \mathbf{x} = (y, x, 0)/2$. Rheological properties of interest are the suspension shear viscosity is $\eta_{eff} = \eta\,(1+\phi S_{xy})$ and normal stress differences, $N_1 = \phi(S_{xx} - S_{yy})$ and $N_2 = \phi(S_{yy} - S_{zz})$.

## ELECTRORHEOLOGY OF A DILUTE EMULSION

Analytical solutions are available in the limit of small drop deformations. An electric field applied in a direction perpendicular to the shear flow (along the velocity gradient) modifies the emulsion stresses depending on the flow conditions.

### Weak flows: $Ca_{\dot\gamma} \ll 1$ with $\lambda = O(1)$

Shear viscosity is unaffected and normal stresses arise solely from the electric field

$$S_{xy} = \frac{5\lambda + 2}{2(\lambda + 1)}, \quad N_1 = -N_2 = \phi Mn \frac{27(R - S)}{5(\lambda + 1)(R + 2)^2}$$

where $Ca_{\dot\gamma} = \eta\dot\gamma a/\gamma$ and $Mn = Ca/Ca_{\dot\gamma} = \varepsilon E_0^2/\eta\dot\gamma$, $\dot\gamma$ is the shear rate.

### High viscosity drops and weak flow, $\lambda, Ca^{-1} \gg 1$

Both shear viscosity and normal stresses are shear-rate dependent

$$S_{xy} = \frac{5}{2} + \lambda^{-1}\left[-\frac{25}{4} + \frac{19}{4[1 + (19\bar{Ca}/20)^2]}\left(1 + \bar{Ca}_{\rm el} G\left(R, S, \bar{Ca}\right)\right)\right] + O\left(\lambda^{-2}, \lambda^{-1} Mn\right)$$

where $\bar{Ca} = \lambda^{-1}\eta\dot\gamma a/\gamma$ is the dimensionless shear rate and $\bar{Ca}_{\rm el} = \lambda^{-1} Ca$. In the absence of electric field, $Ca_{\rm el} = 0$, the emulsion is shear thinning. The electric field can cause either shear-thinning or shear-thickening depending on $R$ and $S$:

$$G\left(R, S, \bar{Ca}\right) = \frac{9\left(2528 + 361\bar{Ca}^2\right)\left(5R^2 + 9R - 19S + 5\right)}{212800(2 + R)^2}.$$

The corresponding expressions for the normal stresses can be found in (Vlahovska et al. 2009a).

The effects of electric fields on emulsion flow have been studied only to a limited extent experimentally (Ha & Yang 2000b, Pan & McKinley 1997, Tadavani et al. 2016, Varshney et al. 2016) and via numerical simulations (Fernandez 2008a,b). Analytical solutions for the emulsion rheology were developed by (Mandal & Chakraborty 2017a,c, Vlahovska et al. 2009a) in the limit of small drop deformations and are summarized in the sidebar titled *Electrorheology of a dilute emulsion*. These results show that application of an electric field perpendicular to the shear flow gives rise to normal stresses and may lead to shear–thickening or –thinning depending on the electric properties of the fluids. In weak flows, the effects of electric field and external shear flow are additive: the shear viscosity is constant and given by (Taylor 1932) for spherical drops; the normal stresses are only due to the electric field. In the case of high-viscosity drops, drop rotation couples the shear– and electric–field–induced deformation leading to shear-rate dependent viscosity and normal stresses. For an electric field applied in the velocity gradient direction, emulsion viscosity depends on the drop polarization, e.g., $R/S > 1$ leads to prolate deformations, greater resistance to the applied shear and hence increase in effective viscosity (PER). In the opposite

case, $R/S < 1$, drops adopt oblate spheroidal shapes, which offer less resistance to the imposed flow and therefore the viscosity decreases (NER).

## 3.3. Drop dynamics in strong electric fields

Drop response to strong electric fields ($Ca \gtrapprox 1$) depends on $R/S$ (the ratio of charge relaxation times).

**3.3.1. Prolate drops, $R/S > 1$.** Drops with $R/S >$ elongate in the direction of the applied field. The shapes are described using models assuming ellipsoidal (Nganguia et al. 2013, Zabarankin 2013, Zhang et al. 2013a) or slender, cigar-like shapes (Yariv & Rhodes 2013). Above a critical field strength, the prolate drop eventually disintegrates (Karyappa et al. 2014, Lac & Homsy 2007, Pillai et al. 2016). Two main modes of break-up have been identified: (*i*) end pinching, where the drop develops bulbous ends that eventually detach, and (*ii*) electrohydrodynamic streaming (or cone-jetting), where the drop develops conical tips (Taylor cones) emitting thin jets (Collins et al. 2008, 2013, de la Mora 2007, Ganan-Calvo et al. 2016), see Figure 1. The mode selection has a complex dependence on the system physical parameters, such as viscosity ratio $\lambda$, and field strength, $Ca$. Inertia and surface charge convection can also play significant role. For example, (Sengupta et al. 2017) recently found via simulations that charge convection can cause transition in the drop breakup mode from end pinching to formation of conical ends.

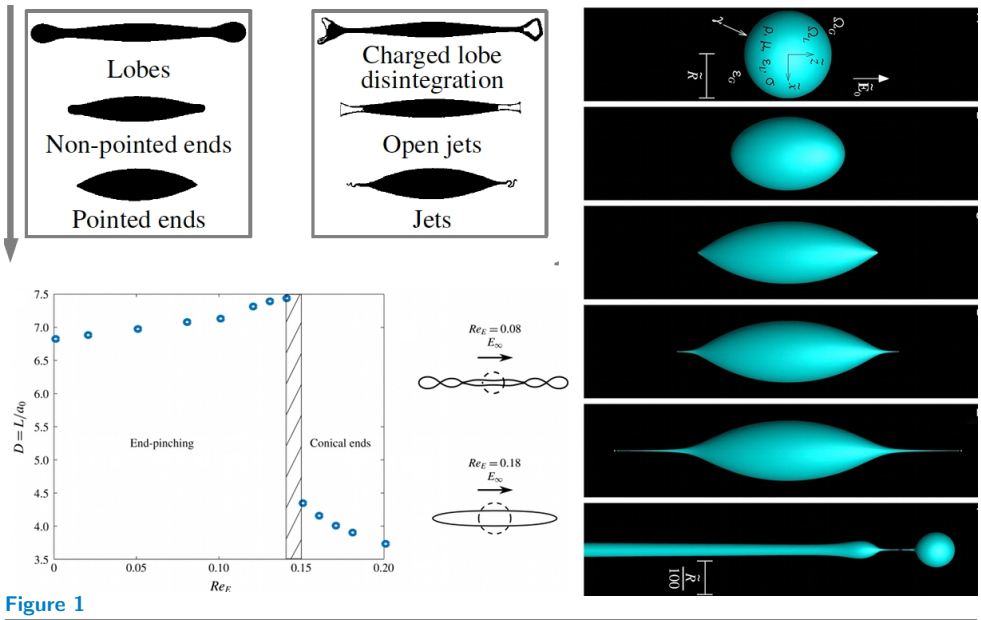


**Figure 1**

(a) Images of different types of shapes of a conducting drop suspended in a dielectric oil (Karyappa et al. 2014). (b) Numerical simulations of EHD tip streaming (Collins et al. 2013). The last snapshot zooms into the about-to-form electrospray droplet. (c) Transition from end-pinching to tip-streaming mode with increasing charge convection as observed in simulations (Sengupta et al. 2017) .

**3.3.2. Oblate drops, $R/S < 1$.** The dynamics of oblate drops in strong fields is illustrated in Figure 2 on the example of a silicone oil drop in castor oil. There are three distinct modes:

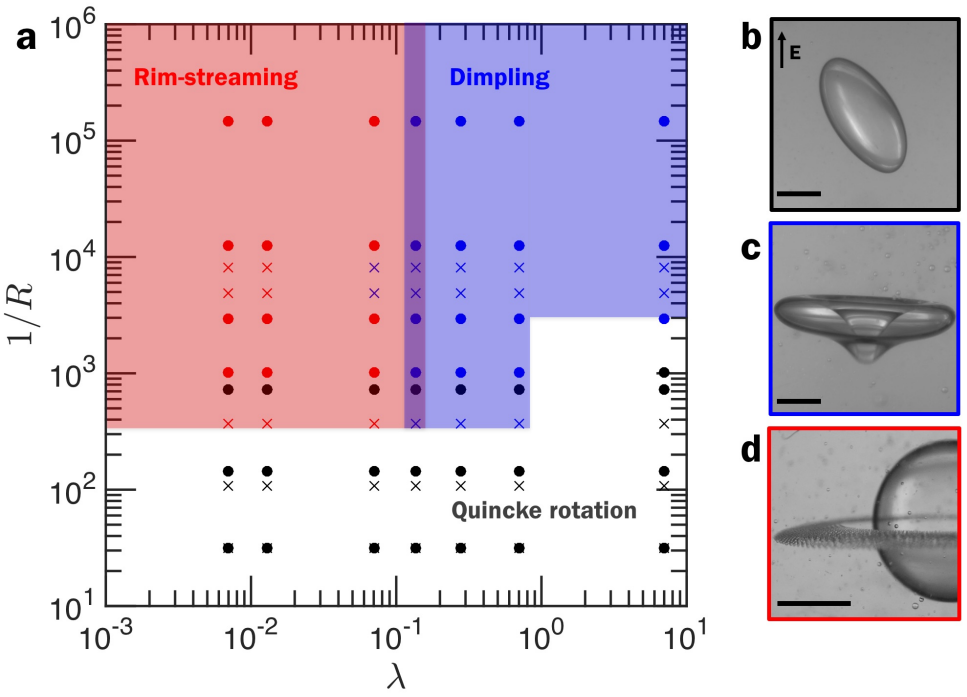


**Figure 2**

Oblate drop dynamics in a strong uniformDC electric field: Quincke electrorotation (black, image (b)), dimpling (blue, image (c)) for $\lambda > 0.1$, EHD equatorial streaming (red, image (d)) for $\lambda < 0.1$. (Brosseau & Vlahovska 2017)

(*i*) *Electrorotation* ($Ca > Ca_Q$, any viscosity ratio $\lambda$): In this regime, the drop tilts relative to the applied field direction. This symmetry-breaking is due to Quincke electrorotation (Ha & Yang 2000a, Salipante & Vlahovska 2010, 2013, Tyatyushkin 2017, Vlahovska 2016, Yariv & Frankel 2016), see Section 3.3.3.1, which gives rise to a rotational flow about the drop. The Quincke effect suppresses drop deformation and stabilizes the drop against break-up (Das & Saintillan 2017a, He et al. 2013). The threshold for electrorotation, $E_Q$ is estimated from the value for a rigid sphere (Jones 1984) (see Section 3.3.3.1)

$$E_Q^2 = \frac{2\sigma\eta\,(R+2)^2}{3\varepsilon^2(S-R)}\,. \tag{18.}$$

(*ii*) *Dimpling* ($R \ll 1$, $Ca \approx 1$, $\lambda \gtrapprox 0.1$): In this mode, the drop deforms into a biconcave disc with rounded rim and pinches in its center to form a torus; the torus subsequently breaks into several, relatively large drops (Ghazian et al. 2014, Pairam & Fernández-Nieves 2009, Torza et al. 1971). The critical capillary number for dimpling is $Ca \sim O(1)$, corresponding to distorting electric stresses overcoming the interfacial tension. The dimpling behavior for viscosity ratios $\lambda \gtrapprox 1$ has been seen also in numerical simulations (Lac &

Homsy 2007, Zabarankin et al. 2013).

(*iii*) *Equatorial streaming* ($R \ll 1$, $Ca \gg 1$, $\lambda \leq 0.1$): In this recently discovered mode, the drop flattens and forms a sharp edge with thin film attached to it (edge-sheet), see Figure 3(Brosseau & Vlahovska 2017). The edge sheet emits concentric thin rings which break up into microdroplets. The ring shedding occurs in a steady manner and microdroplet production has been observed for tens of seconds. The equatorial streaming is likely related

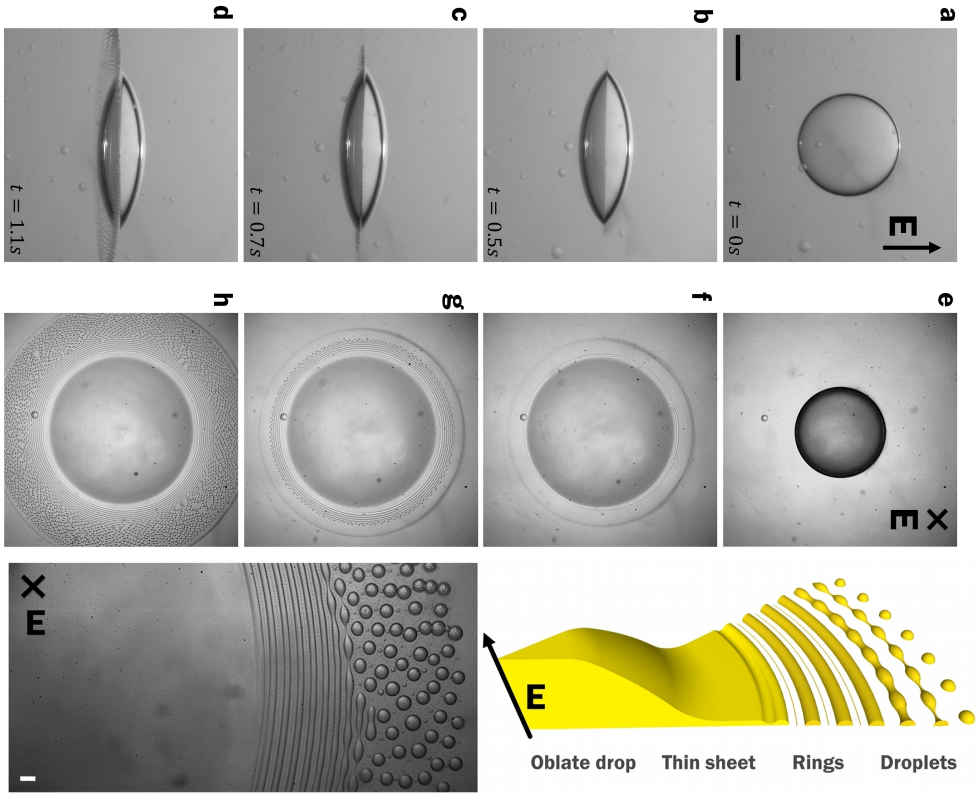


**Figure 3**

EHD equatorial streaming (A) observed from direction perpendicular (a-d) and along (e-h) the applied electric field; the field direction is the axis of symmetry. (B)Close up and rendering of the phenomenon as deduced from the experiment.

to the interfacial instabilities common in convergent flow (Tseng & Prosperetti 2015). The interface is compressed and a local perturbation at the stagnation line (the drop equator) gets drawn out by the flow. When the viscous stresses overcome the interfacial tension, the perturbation grows into a fluid sheet. This is similar to the tip streaming phenomenon commonly observed in the microfluidic co-flow geometry (Anna 2016, Castro-Hernandez et al. 2012, Suryo & Basaran 2006), where a fluid filament is formed at a stagnation point. However, inertia may also play role: Schnitzer et al. (2013a) suggest with analysis two boundary layers propagate from the poles to the equator, where they collide to form a radial jet.

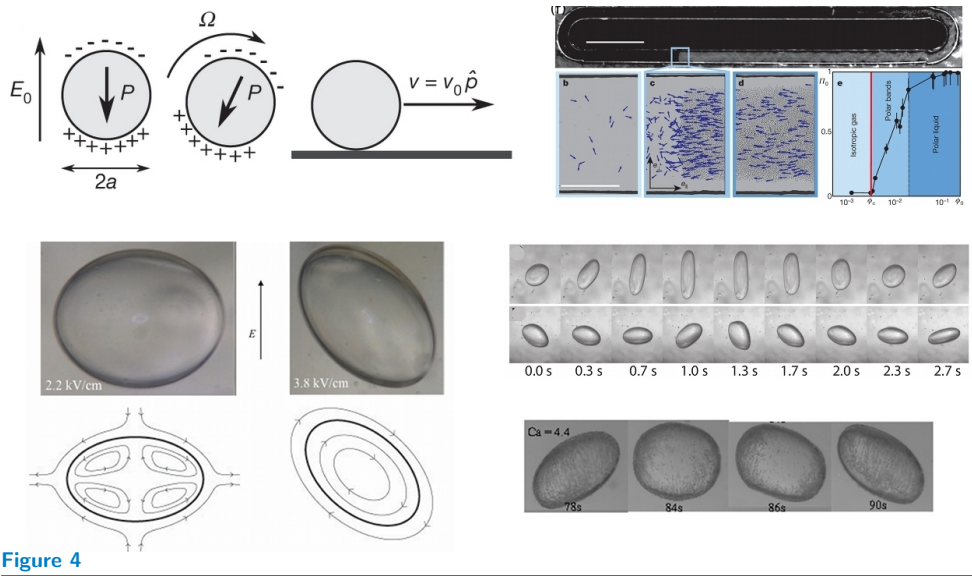


**Figure 4**

A. Charge distribution in unstable equilibrium for a sphere with $R/S < 1$. Above a critical field strength $E_0 > E_Q$ , where $E_0 = |\mathbf{E}|$ and $E_Q$ is given by Eq. 18, constant rotation around an axis perpendicular to the electric field is induced by the misaligned dipole moment of the particle. If the sphere is initially resting on a surface, it rolls. Population of Quincke-rollers self-organize in a band propagating along the "racetrack". The arrows correspond to the rollers velocities. (Bricard et al. 2013). B. Sketches illustrating drop shape and flow streamlines in a uniform direct current (DC) electric field in the Taylor regime ($E < E_Q$, axisymmetric compressional flow and oblate shape) and the Quincke regime $E \geq E_Q$ ( rotational flow and the drop is tilted with respect to the applied field direction. (Salipante & Vlahovska 2010). C. In even stronger fields, the drop undergoes unsteady dynamics depending on the viscosity ratio: drop tumbles ($\lambda \gg 1$) or "breathes" as it rotates ($\lambda \sim 1$). Experimental system is silicon oil drop suspended in castor oil (Ouriemi & Vlahovska 2014, Salipante & Vlahovska 2013).

**3.3.3. Electrorotational instabilities of oblate drops.** While in weak fields the electrohydrodynamic flow induced by a uniform field is axisymmetric about the applied field direction, in strong fields and if $R/S < 1$ the flow can undergo symmetry-breaking.

***3.3.3.1. Quincke rotation.*** The spontaneous spinning of a rigid sphere in a uniform DC electric field has been known for over a century (Lemaire & Lobry 2002, Melcher & Taylor 1969). This phenomenon has enjoyed a resurgence of interest recently as a mechanism to "activate" particles for self-propulsion (Bricard et al. 2013, Kokot et al. 2017, Lavrentovich 2016, Snezhko 2016, Yeo et al. 2015).

For rotation to occur, the induced dipole moment of the sphere, listed in the sidebar titled *A Sphere in a Uniform Electric Field*, has to orient opposite to the applied field, which requires $R/S < 1$. This configuration is unfavorable and becomes unstable above a critical strength of the electric field. A perturbation misaligns the dipole and the applied field, and the resulting torque induces rotation around an axis perpendicular to the applied field direction.

For rotation to be sustained, the rotation and the dipole evolution should take place on comparable time scales. This condition ensures that while the induced free surface charge rotates with the sphere, the exterior fluid can recharge the interface. The balance between

surface charge convection by rotation and supply by conduction from the bulk is given by (Lemaire & Lobry 2002)

$$\Omega P_{||} = t_{\rm mw}^{-1} P_\perp \,, \quad \Omega P_\perp = t_{\rm mw}^{-1} \left[ P_{||} - \left( P^{AC}(0) - P^{AC}(\infty) \right) E \right] . \tag{19.}$$

The rotation rate $\Omega$ of the Quincke rotor is determined from the balance of electric and viscous torques on the sphere (Jones 1984, Turcu 1987)

$$P_\perp E = 8\pi\eta a^3 \Omega \,, \tag{20.}$$

Steady state solutions of Eq. 20 and Eq. 19 are no rotation($\Omega = 0$, $P_\perp = 0$, and induced dipole $P_{||}$ given in the sidebar *A sphere in a uniform electric field*), and steady rotation with an oblique dipole orientation illustrated in Figure 4

$$\Omega = \pm \frac{1}{t_{\rm mw}} \sqrt{\frac{E_0^2}{E_Q^2} - 1} \,, \quad P_\perp = \frac{8\pi\eta a^3 \Omega}{E_0} \,, \tag{21.}$$

where the $\pm$ sign reflects the two possible directions of rotation and $E_Q$ is given by Eq. 18. Eq. 21 shows that rotation is possible only if the electric field exceeds a critical value given by $E_Q$.

Drop electrorotation is more complex, due to deformation and electrohydrodynamic flow. The experiments show that the deformed droplet can assume a steady tilted orientation relative to the applied field (Ha & Yang 2000a, He et al. 2013, Salipante & Vlahovska 2010) or undergo irregular rotational motions (Salipante & Vlahovska 2013, Sato et al. 2006), see Figure 4. The threshold for electrorotation increases and shows hysteresis as drop viscosity decreases (Salipante & Vlahovska 2010).

The steady tilt is well understood (Das & Saintillan 2013, He et al. 2013, Yariv & Frankel 2016). Analytical models, which assume small-deformations and charge convection dominated by the rotational flow, agree with the experimental data for high viscosity drops (He et al. 2013). However, these models do not capture the increased threshold of electrorotation and unsteady dynamics of low-viscosity drops that likely arise from charge convection due to the straining flow and anisotropy in the polarization relaxation due to the non-spherical shape (Salipante & Vlahovska 2013). Indeed, the electrorotation dynamics of rigid ellipsoids is richer, and includes swinging and tumbling (Brosseau et al. 2017, Cebers et al. 2000, Dolinsky & Elperin 2009). Including shape variations as observed in the case of the low-viscosity drop is analytically challenging and tractable only by fully three-dimensional numerical simulations. Such simulations are currently unavailable as nearly all three dimensional computational analyses of drop electrohydrodynamics are restricted to axisymmetric geometries (Dubash & Mestel 2007, Lac & Homsy 2007, Lanauze et al. 2015, Nganguia et al. 2015, Pillai et al. 2016)) with exception of (Das & Saintillan 2017a), which however is limited to high viscosity drops.

***3.3.3.2. Equatorial vortices.*** Another electrorotation-like phenomenon is the formation of particle vortices along the equator of a particle-coated drop, see Figure 5, (Dommersnes et al. 2013, Ouriemi & Vlahovska 2014, 2015, Rozynek et al. 2015, 2014). The mechanism responsible for the belt break-up into rotating clusters is presently unknown. It is not clear if this is a result of (i) self-organization emerging from the collective particle dynamics or (ii) a purely hydrodynamic instability occurring even in the absence of particles.

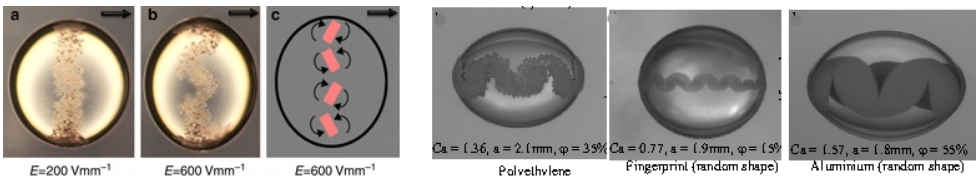


**Figure 5**

a-c Colloidal particles adsorbed on a drop interface accumulate at the equator and form a belt, which breaks into rotating clusters of particles (Dommersnes et al. 2013). d-f: Vortices formed by different kind of particles (Ouriemi & Vlahovska 2014).

Self-organization is supported by a simple model of particles trapped on the drop interface (Yeo et al. 2015) . Numerical simulations of the collective dynamics of a monolayer of spheres driven by constant clockwise or counterclockwise torques showed the emergence of patterns resembling those seen in experiments.

Supporting an instability, a cellular interfacial flow in the form of rolls has been observed in the case of an uniform electric field imposed tangentially to a nearly planar interface (Malkus & Veronis 1961). The charge distribution on a drop near the equator is similar to this unstable configuration. Malkus & Veronis (1961) analysis (assuming negligible charge convection and instantaneous polarization) shows that the induced charge depends on the slope of the interfacial profile

$$Q = \varepsilon E \frac{2\,(S-R)}{(R+1)} \frac{dh}{dx}, \qquad 22.$$

where $R$ and $S$ are the ratios between the top/bottom fluids (corresponding to drop/suspending fluids) and $h(x)$ is the surface shape. If $R/S < 1$ the charge distribution is such that a perturbation above a critical $E$ field could set-up a steady cellular flow, akin to Quincke rotation.

## 4. VESICLES

The electro-deformation of giant vesicles (cell-sized closed membranes made of lipid bilayers, usually about 20 $\mu$m diameter) provides fundamental insights into the electromechanics of biomembranes, namely the coupling of membrane shape and transmembrane potential (Dimova et al. 2009, Perrier et al. 2017, Portet et al. 2012, Vlahovska 2015). Experiments with vesicles in a spatially uniform electric field reveal morphological changes that closely mimic cell behaviors, e.g., deformation into a spheroid (Aranda et al. 2008, Riske & Dimova 2005, Salipante et al. 2012, Salipante & Vlahovska 2014), pearling of a tubular vesicle (Sinha et al. 2013), and phase–separation ("raft" formation) in multicomponent membranes (Salipante et al. 2015). Other intriguing dynamics have also been observed: lipid flows and mixing (Staykova et al. 2008), wrinkling (Knorr et al. 2010), and burst (Riske et al. 2009). Electroporation and pore closure has been recently utilized as a method to measure edge tension (Portet & Dimova 2010). Figure 6 illustrates some of the behaviors of a quasi-spherical vesicle exposed to a uniform electric field

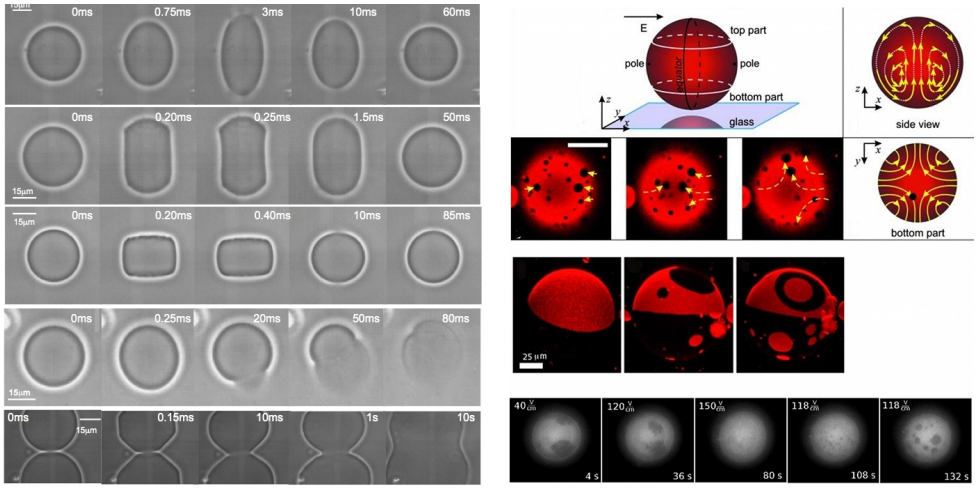


**Figure 6**

A. Vesicle response in a square DC pulse. a). Deformation and poration. Pulse duration 200 $\mu s$. (Riske & Dimova 2005). The suspending fluid is salt–free. b),c) "Squaring" Vesicle in salt solution deforms into a spherocylinder with long axis parallel and perpendicular to the field depending on the conductivity ratio of the inner and outer solutions. b- $R > 1$ c- $R < 1$. d). Vesicle burst (Riske et al. 2009). e). Vesicle electrofusion induced by 150 $\mu s$ DC pulse (Haluska et al. 2004). B. a) Alternating electric (AC) fields induce circular patterns of lipid transport in membranes of giant vesicles. The flow is visualized by fluorescently labelled lipid domains. (Staykova et al. 2008). The yellow dashed arrows indicate the trajectories of selected domains. b). 3D confocal scans of the lower vesicle hemisphere illustrating lipid mixing induced by AC field. Before applying the field, the vesicle has only two domains, which break apart after continuous field exposure of 2 min and 3 min. c). Domain dissolution and reappearance upon increase and decrease of electric field strength (Salipante et al. 2015).

## 4.1. Electromechanics of the vesicle membrane

The thickness of the lipid bilayer (about 5 nm) is much smaller than the typical giant vesicle size (radius of about 10 $\mu$m). Accordingly, the membrane can be treated as a two–dimensional surface embedded in a three–dimensional space.

**4.1.1. The vesicle membrane is a capacitive interface.** In contrast to fluid-fluid interfaces, the lipid bilayer is impermeable to ions, so in an electric field it acts as a capacitor. The accumulation of ions at the membrane surfaces sets up a potential difference across the membrane, $\hat{\Phi} - \Phi = V_{\rm mm}$. The charging of the membrane capacitor modifies the current balance equation Eq. 6 (DeBruin & Krassowska 1999, Grosse & Schwan 1992, Seiwert et al. 2012)

$$C_{\rm mm}\frac{dV_{\rm mm}}{dt} + G_{\rm mm}V_{\rm mm} = \sigma\mathbf{n}\cdot\mathbf{E} = R\sigma\mathbf{n}\cdot\hat{\mathbf{E}}\,. \qquad 23.$$

where $C_{\rm mm}$ is the membrane capacitance and $G_{\rm mm}$ is the membrane ohmic conductance (e.g., due to pores and ion channels or pumps). Charge convection is neglected. The charging dynamics obtained from Eq. 23 in the case of a spherical capacitor is illustrated in Figure 7 and the main results are summarized in the sidebar titled *A spherical vesicle in a uniform DC electric field*. Vesicle deformation is strongly affected by the capacitive

charging.

- At short times (or equivalently, intermediate frequencies in an AC field) $t \ll t_{\rm mm}$ ($\omega > \omega_c$) the membrane capacitor is short-circuited and there is charge imbalance between the inner and outer membrane surfaces. If the enclosed solution is more conducting than the suspending fluid, $R > 1$, the vesicle is pulled into a prolate ellipsoid. The polarization is reversed in the opposite case, $R < 1$, and the vesicle deforms into an oblate ellipsoid.
- At long times (or similarly for low frequencies in an AC field) $t \gg t_{\rm mm}$ ($\omega < \omega_c$) the membrane capacitor is fully charged and vesicle shape is an prolate ellipsoid at any $R$.

A vesicle with $R < 1$ subjected to a DC uniform field may initially deform into an oblate spheroid but eventually adopts a prolate shape (Salipante & Vlahovska 2014, Schwalbe et al. 2011b). Similar transition in an AC field is readily observed by lowering the field frequency (Aranda et al. 2008, Vlahovska et al. 2009b) below a critical value $\omega_c$ (Yamamoto et al. 2010)

$$\omega_c = \frac{\sigma}{aC_{\rm mm}}\left[(1-R)(R+3)\right]^{-1/2}. \qquad 24.$$

For systems with typical solution conductivity $\sigma \sim 0.1\mu$S/cm, $a \sim 10\mu$m and membrane capacitance $C_{\rm mm} \sim 1\mu F/cm^2$ the charging timescale is $t_{\rm mm} \sim 1$ms and $\omega_c \sim 1kHz$. For applied electric field of $E \sim 1kV/cm$, $V_{\rm mm}$ is around $1V$.

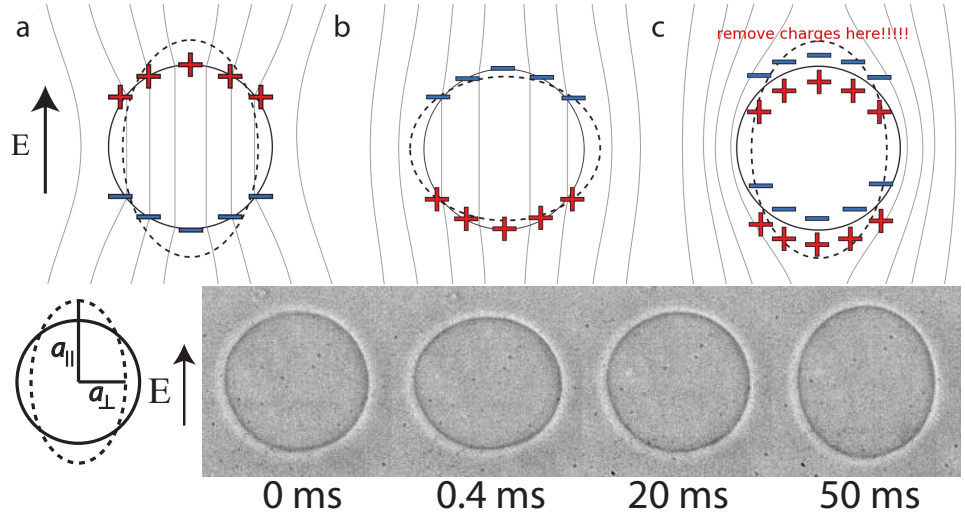


**Figure 7**

(A) Electric field lines and net charge distribution at the interface as the membrane capacitor charges (a) $R > 1$, and (b) $R < 1$. (c) At long times, if the membrane is perfectly insulating $G_{\rm mm} = 0$, the electric potential is uniform and $\hat{\mathbf{E}} = 0$ in the vesicle interior and deformation is independent of the conductivity ratio $R$. Note that since the enclosed and suspending fluids are aqueous solutions $S \approx 1$. The dashed lines indicate the vesicle deformation. (B) Shape evolution of a vesicle in a DC field illustrating the oblate-prolate transition for $R < 1$(Salipante & Vlahovska 2014)

## A SPHERICAL VESICLE IN A UNIFORM DC ELECTRIC FIELD

The vesicle is modeled as a spherical capacitor of radius $a$. The potential jump between the inner and outer membrane surfaces is

$$V_{\rm mm}(t) = aE_0\bar{V}(t)\cos\theta\,,$$

where $\theta$ is the angle between the electric field direction and position at the interface. The time dependence after application a uniform DC field, $\mathbf{E} = E_0\hat{\mathbf{z}}\,, t > 0$,is

$$\bar{V}(t) = \frac{3}{2\left(1 + G_{\rm mm}\left(\frac{1}{2} + \frac{2}{R}\right)\right)}\left(1 - e^{-t/t_{\rm mm}}\right)\,,$$

where the capacitor charging time is

$$t_{\rm mm} = \frac{aC_{\rm mm}}{\sigma}\frac{(2+R)}{2R + G_{\rm mm}(2+R)}\,.$$

The electric potential is described by (Schwalbe et al. 2011b, Vlahovska 2010)

$$\Phi = -aE_0\left(r + P(t)r^{-2}\right)\cos\theta\,, \quad \hat{\Phi} = -aE_0\hat{P}(t)r\cos\theta$$

where

$$P(t) = \frac{1 - R + R\bar{V}(t)}{2+R}\,, \quad \hat{P}(t) = \frac{3 - 2\bar{V}(t)}{2+R}\,.$$

**4.1.2. The vesicle membrane is a flexible, area-incompressible fluid interface.** The lipid bilayer contains a fixed number of molecules, which are free to move within the membrane. True stretching (increase per area of lipid) occurs only at very high stresses; the lipid membrane fails above area strain of 4 % (Evans & Rawicz 1990). Accordingly, the lipid bilayer can be treated as an incompressible two-dimensional fluid. The tension, $\Sigma$, is not a material property (unlike the surface tension of fluid-fluid interfaces) but a Lagrange multiplier enforcing the local area incompressibility. Under stress, the bilayer responds by (i) bending rather than stretching, and (ii) developing nonuniform tension, which adapts itself to the forces exerted on the membrane in order to keep the local area constant.

The interfacial stresses according to the standard Helfrich membrane model (Seifert 1997) are

$$\mathbf{t}^{\rm mm} = \kappa\left(4H^3 - 4KH + 2\nabla_s^2 H\right)\mathbf{n} + 2\Sigma H\mathbf{n} - \nabla_s\Sigma\,, \qquad 25.$$

where $H = -\frac{1}{2}\nabla_s\cdot\mathbf{n}$ is the mean curvature and $K$ is the Gaussian curvature. Membranes are very soft, $\kappa$ is about $10k_BT$, where $k_BT \sim 10^{-21}$ J is the thermal energy. At equilibrium, the membrane tension is uniform and low, $\Sigma \sim 10^{-9} - 10^{-6}$ N/m. As a result of the low bending rigidity and tension, vesicle shapes fluctuate due to thermally driven membrane undulations.

Area–incompressibility implies that the total area $A$ of a vesicle is constant. Hence, a spherical vesicle can not deform, because the sphere is a shape with minimum area. The vesicle must be non-spherical in order to deform. The vesicle asphericity is characterized

by the excess area $\Delta$, $A = a^2(4\pi + \Delta)$; the total excess area $\Delta$ is a fixed parameter for a given vesicle.

Vesicles, however, even though appearing spherical under the microscope, deform under stress (an example of such deformations in an electric field are shown in Figure 7.B). The increase of apparent area, $a^2(4\pi + \bar{\Delta})$, comes from smoothing suboptical membrane undulations. During vesicle deformation, the (fixed) total area, $\Delta$, gets redistributed between the experimentally measured apparent area, $\bar{\Delta}$ and the area stored in shape fluctuations, $\Delta_f$, $\Delta = \bar{\Delta} + \Delta_f$. The latter is (Seifert 1999)

$$\Delta_f\left(\bar{\Sigma}\right) = \frac{k_B T}{2\kappa} \ln\left(\frac{j_{max}^2 + j_{max} + \bar{\Sigma}}{6 + \bar{\Sigma}}\right) \approx \frac{k_B T}{2\kappa} \ln\left(\frac{j_{max}^2}{\bar{\Sigma}}\right), \tag{26.}$$

where $j_{max} = a/d \sim 1000$ is the ratio of the vesicle radius to the membrane thickness and $\bar{\Sigma} = \Sigma a^2/\kappa$ is the membrane tension. The approximation is valid in the so called "entropic regime" $j_{max}^2 \gg \bar{\Sigma} \gg 6$.

The membrane tension is coupled to the excess area and varies during vesicle deformation. For a quasi-spherical vesicle, whose apparent excess area at equilibrium is $\bar{\Delta} = 0$ Eq. 26 in the entropic regime yields the widely used relation (Seifert 1997)

$$\bar{\Sigma} = \bar{\Sigma}_0 \exp\left(\frac{2\kappa}{k_B T}\bar{\Delta}\right), \tag{27.}$$

where $\Sigma_0$ is the equilibrium tension. This equation can be used to study the relaxation of a deformed vesicle towards its equilibrium (apparently) spherical shape (Yu et al. 2015).

## 4.2. Vesicle deformation in a uniform electric field

The shapes of vesicles in uniform AC and DC fields have been analyzed theoretically (Ngan-guia et al. 2013, Schwalbe et al. 2011b, Vlahovska et al. 2009b, Yamamoto et al. 2010, Zhang et al. 2013b) and numerically (Kolahdouz & Salac 2015a,b, McConnell et al. 2013, 2015a,b, Veerapaneni 2016) .

Using the spherical harmonic parametrization introduced in Section 3.1, the shape evolution of a quasi-spherical vesicle is described by

$$\frac{\partial f_{jm}}{\partial t} = j(1+j)\frac{(\tau^{\rm el}_{jm2} + \tau^{s}_{jm2}) + 2(\tau^{\rm el}_{jm0} + \tau^{s}_{jm0})}{2j^3 + 3j^2 + 4 + 4\left(j^2 + j - 2\right)\lambda^{\rm mm}_{\eta} + \left(2j^3 + 3j^2 - 5\right)\lambda}. \tag{28.}$$

This equation is the analogue of the shape evolution Eq. 9 for drops. The expression is, however, simpler due to the area-incompressibility. The surface stresses are

$$\tau^{s}_{jm0} = 0, \quad \tau^{s}_{jm2} = -\mathcal{B}^{-1}(j-1)(j+2)\left(j(j+1) + \bar{\Sigma}\right) f_{jm}, \tag{29.}$$

where $\mathcal{B} = \eta E_0^2 a^3/\kappa$ and $\bar{\Sigma} = \Sigma a^2/\kappa$. In a uniform electric field, the electric stresses are

$$\tau^{\rm el}_{202} = \frac{1}{3}\left(2 - 2S\hat{P}(t)^2 - 2P(t) + 5P(t)^2\right), \quad \tau^{\rm el}_{200} = \frac{1}{3}\left(1 - S\hat{P}(t)^2 - P(t) - 2P(t)^2\right), \tag{30.}$$

where $P(t)$ is the induced dipole coefficient (see the sidebar titled *A spherical vesicle in a uniform direct current electric field*). Because in the case of vesicles $P(t)$ and $\hat{P}(t)$ depend on the potential discontinuity $V_{\rm mm}(t)$, the electric stresses are different than the ones for drops. Only if the membrane is highly conducting $G_{\rm mm} \gg 1$ does $V_{\rm mm} = 0$ and the electric

stresses are the same as the one derived in Section 3.1, Eq. 14. The shape evolution derived from Eq. 28 is listed in the sidebar titled *Vesicle deformation in a square electric pulse*.

A difference between the modeling of the deformation dynamics of vesicles and drops is the treatment of the tension. While for drops the tension a material property, for vesicles the membrane tension $\bar{\Sigma}$ needs to be determined self-consistently with deformation because of its dependence on the apparent excess area discussed in Section 4.1.2 (Seifert 1999). Under stress, a quasi-spherical vesicle deforms by pulling excess area stored in fluctuations. The area constraint requires that the total excess area $\Delta$ (stored in fluctuations, $\Delta_f$, and apparent deformation, $\bar{\Delta}$) is constant. Accordingly, given $\Delta$, $\Delta = \bar{\Delta} + \Delta_f$ must be solved numerically at each time step to determine $\bar{\Sigma}$. $\Delta_f$ is calculated from Eq. 26. The excess area corresponding to the apparent deformation is calculated form the shape modes $f_{jm}$ as

$$\bar{\Delta} = \sum_{j=2}^{jmax} \sum_{m=-j}^{j} \frac{(j+2)\,(j-1)}{2} \bar{f}_{jm} \bar{f}^*_{jm}\,, \tag{31.}$$

where $\bar{f}_{jm}$ solves Eq. 28 with $\partial f_{jm}/\partial t = 0$.

## VESICLE DEFORMATION IN A SQUARE ELECTRIC PULSE

The shape is an axisymmetric ellipsoid parametrized by $r_s = a(1 + s(t)P_2(\cos\theta))$. The shape evolution is described by

$$\frac{\partial s}{\partial t} = \frac{24}{32 + 23\lambda + 16\lambda_\eta^{\rm mm}} \left(C(t) - \mathcal{B}^{-1}(6 + \bar{\Sigma})s(t)\right),$$

where the forcing term is

$$C(t) = \frac{1}{12(2+R)^2}\left[9(1+R)^2 - 36S - 6(R + R^2 - 8S)\bar{V}(t\delta_m) + (R^2 - 16S)\bar{V}^2(t\delta_m)\right]$$

and $\bar{V}(t)$ is listed in the sidebar A spherical vesicle in a uniform DC electric field. For an insulating membrane, $G_{\rm mm} = 0$,

$$\bar{V}(\tau) = \frac{3}{2}\left(1 - e^{-\tau}\right),$$

Note that time is nondimensionlaized by the electrohydrodynamic time-scale $t_c$; $\delta_m = t_c/t_{\rm mm}$ is the ratio of the electrohydrodynamic and capacitor charging time scales.

Unlike emulsions, the electrorheology of vesicle suspensions has not been studied experimentally. Only few studies address the dynamics of vesicles in a combined electric field and shear flow. The contribution to the effective viscosity of a dilute suspension of vesicles is predicted to be (Vlahovska 2016)

$$S_{xy} = \frac{5}{2\left(23\hat{\lambda} + 32\right)}\left[23\hat{\lambda} - 16 + 48\left(\Lambda \sin(2\psi)\right)^2\right]. \tag{32.}$$

$\hat{\lambda} = \lambda + 16\lambda_\eta^{\rm mm}/23$ is the effective viscosity ratio which accounts for both bulk and membrane viscosities, $\psi$ and $\Lambda$ are calculated from the shape parameters as $f_{2m} = \frac{\sqrt{\Delta}}{2}\Lambda \exp(-im\psi)$. $\psi$ is the angle between the vesicle major axis and the flow direction. Eq. 32 shows that

the effective viscosity of the vesicle suspension depends on the vesicle orientation relative to the flow, $\psi$, which is determined by the competition of the flow and electric field torques (Schwalbe et al. 2011b).

## 4.3. Membrane instabilities

Electric pulses are used deliver exogenous molecules (such as drugs and DNA) into living cells. The electric stresses create pores in the cell membrane, through which the molecules enter the cell. Ideally, these pores should reseal after the field is turned off. However, often the membrane collapses leading to cell death.

The mechanisms of membrane poration and collapse have been investigated using linear stability analyses. Earlier models have mainly focused on thickness fluctuations (peristaltic modes) (Weaver & Chizmadzhev 1996). The bending (undulation) modes were also found to be unstable (Lacoste et al. 2007, Schwalbe et al. 2011a, Sens & Isambert 2002, Young & Miksis 2015, Young et al. 2014).

Equilibrium shape fluctuations with wavenumber $q$ of a planar bilayer membrane separating fluids with viscosity $\eta$ and $\lambda\eta$ are stable with relaxation rate $s(q) = -(\kappa q^3+\gamma q)/2(1+\lambda)\eta$ (Brochard & Lennon 1975, Seifert & Langer 1993). Electric fields affect the membrane undulations (Seiwert et al. 2012, Sens & Isambert 2002, Ziebert & Lacoste 2011). Loubet et al. (2013), Sens & Isambert (2002) showed that the mechanism for that is that electric field induces an effective negative tension in the membrane $-\gamma_m \sim E_0^2$. An instability occurs above a threshold electric field at which the negative tension exceeds the initial tension in the membrane. Another source of instability found by (Lacoste et al. 2007, 2009, Ziebert et al. 2010, Ziebert & Lacoste 2010) is electrokinetic (ICEO) flows near the membrane, which give rise to a positive $q^2$ term in the relaxation rate. However, in the limit of strong electrolytes which have zero Debye thickness this term vanishes and the negative tension is the only source of instability. Most stability analyses considered a membrane separating fluids with the same permittivity and conductivity. In asymmetric system,(Schwalbe et al. 2011a) discovered that a transient instability can develop when the membrane capacitor is charging, e.g., after a step increase in the DC field, if there is difference in the conductivities $R \neq 1$ of the embedding solutions; however, in a steady DC field, a fully charged insulating membrane is linearly stable. In contrast to the purely capacitive membrane, in a steady DC field a conducting membrane is unstable to long-wavelength perturbations if $G_{\rm mm}(R-1)(R^2-S) > 0$ (Seiwert et al. 2012) Furthermore, while an insulating membrane is linearly stable in DC electric fields, in AC fields the membrane can always be made unstable, except for the symmetric case of a membrane separating the same fluids $R = S = 1$ (Seiwert & Vlahovska 2012). At intermediate frequencies ($\omega^{-1} \sim t_{\rm mm}$), where the membrane capacitor is short-circuited, the instability develops when $(R-1)(R^2-S) > 0$.

### SUMMARY POINTS

1. G.I.Taylor' pioneering study of drop electrohydrodynamics derived the steady shape of a drop in a uniform DC electric field. Here, we review the generalization of the Taylor's result to describe the transient response of drops and vesicles to applied electric fields.
2. In strong uniform DC electric field, the axisymmetric flow about drops with $R/S < 1$ can undergo symmetry breaking due to the Quincke rotation effect. The global flow

can acquire rotational component resulting in drop tilt or tumbling; in the case of low viscosity drops, surface electrocovection-like rolls form at the equator. Another instability is the equatorial streaming, which creates visually striking Saturn-rings around the equator of a drop.
3. In the case of vesicles, the capacitive interface gives rise to different dynamics than drops, e.g., oblate-to-prolate shape transition with increasing time/ decreasing frequency. Capacitive charging destabilizes the membrane.

### FUTURE ISSUES

1. The leaky dielectric model neglects diffuse charge and double layers near the interface. The derivation of the LDM from electrokinetic theory for fluid/fluid interfaces is an ongoing effort (Mori & Young 2018, Pascall & Squires 2011, Saville 1997, Schnitzer et al. 2013a,b, Schnitzer & Yariv 2013, Zholkovskij et al. 2002).
2. The mechanisms responsible for the EHD equatorial streaming and vortices are unknown. Numerical simulations to aid undertanding are challenging due to development of charge shocks on the interface (steep charge gradients near the drop equator). An in-depth investigation may reveal additional instabilities.
3. Electrokinetics of particles trapped at interfaces is largely unexplored. There are only few experiments (Zhang et al. 2018), and models of particle motion (Doerr & Hardt 2015) and electrostatic forces on a particle (Danov & Kralchevsky 2013, Hu et al. 2018).
4. Drops with more complex interfaces, e.g., coated with surfactants (Ha & Yang 1995, 1998) or particles (Dommersnes et al. 2013, Mikkelsen et al. 2017, Ouriemi & Vlahovska 2015), are likely to display additional rich electrohydrodynamics and merit further investigation.
5. Vesicles extreme deformations in electric pulses, e.g., the transient sharp edges (Riske & Dimova 2006) and poration (Portet & Dimova 2010), remain poorly understood. The electromechanics of multicomponent membranes, e.g., phase transitions and domain motions, is an important open research area.
6. The effects of electric fields on the collective dynamics and rheology of drops and vesicles are virtually unexplored. A recent numerical study predicts intriguing pairwise interactions and rheology of vesicles in a uniform electric field that warrants further investigation (Wu & Veerapaneni 2018).

## DISCLOSURE STATEMENT

The author is not aware of any affiliations, memberships, funding, or financial holdings that might be perceived as affecting the objectivity of this review.

## ACKNOWLEDGMENTS

I acknowledge financial support from the National Science Foundation grants CBET-1437545, 1748049 and 1704996. I thank Paul Salipante, Jacopo Seiwert, Malika Ouriemi,

Quentin Brosseau, Michael Miksis and Rumiana Dimova for their contributions to this research.

## LITERATURE CITED

Anna SL. 2016. Droplets and Bubbles in Microfluidic Devices. *Annu. Rev. Fluid Mech.* 48:285–309

Aranda S, Riske KA, Lipowsky R, Dimova R. 2008. Morphological transitions of vesicles induced by ac electric fields. *Biophys. J.* 95:L19–L21

Bharti B, Velev OD. 2015. Assembly of Reconfigurable Colloidal Structures by Multidirectional Field-Induced Interactions. *Langmuir* 31:7897–7908

Bricard A, Caussin JB, Desreumaux N, Dauchot O, Bartolo D. 2013. Emergence of macroscopic directed motion in populations of motile colloids. *Nature* 503:95–98

Brochard F, Lennon JF. 1975. Frequency spectrum of the flicker phenomenon in erythrocytes. *J. Phys.(France)* 36:1035–1047

Brosseau Q, Hickey G, Vlahovska PM. 2017. Electrohydrodynamic quincke rotation of an ellipsoid. *Phys. Rev. Fluids* 2:014101

Brosseau Q, Vlahovska PM. 2017. Streaming from the equator of a drop in an external electric field. *Phys. Rev. Lett.* 119:034501

Castro-Hernandez E, Campo-Cortes F, Manuel Gordillo J. 2012. Slender-body theory for the generation of micrometre-sized emulsions through tip streaming. *J. Fluid Mech.* 698:423–445

Cebers A, Lemaire E, Lobry L. 2000. Electrohydrodynamic instabilities and orientation of dielectric ellipsoids in low-conducting fluids. *Phys. Rev. E* 63:016301

Collins RT, Jones JJ, Harris MT, Basaran OA. 2008. Electrohydrodynamic tip streaming and emission of charged drops from liquid cones. *Nature Physics* 4:149–154

Collins RT, Sambath K, Harris MT, Basaran OA. 2013. Universal scaling laws for the disintegration of electrified drops. *PNAS* 110:4905–4910

Danov KD, Kralchevsky PA. 2013. Forces acting on dielectric colloidal spheres at a water/nonpolar-fluid interface in an external electric field. 1. Uncharged particles. *J. Colloid Int. Sci.* 405:278–290

Das D, Saintillan D. 2013. Electrohydrodynamic interaction of spherical particles under Quincke rotation. *Phys. Rev. E* 87:043014

Das D, Saintillan D. 2017a. Electrohydrodynamics of viscous drops in strong electric fields: numerical simulations. *J. Fluid Mech.* 829:127–152

Das D, Saintillan D. 2017b. A nonlinear small-deformation theory for transient droplet electrohydrodynamics. *J. Fluid Mech.* 810:225–253

de la Mora JF. 2007. The fluid dynamics of taylor cones. *Ann. Rev. Fluid. Mech.* 39:217–243

DeBruin KA, Krassowska W. 1999. Modeling electroporation in a single cell. i. effects of field strength and rest potential. *Biophys. J.* 77:1213–1224

Deshmukh SD, Thaokar RM. 2013. Deformation and breakup of a leaky dielectric drop in a quadrupole electric field. *J. Fluid Mech.* 731:713–733

Dimova R, Bezlyepkina N, Jordo MD, Knorr RL, Riske KA, et al. 2009. Vesicles in electric fields: Some novel aspects of membrane behavior. *Soft Matter* 5:3201 – 3212

Dobnikar J, Snezhko A, Yethiraj A. 2013. Emergent colloidal dynamics in electromagnetic fields. *Soft Matter* 9:3693–3704

Doerr A, Hardt S. 2015. Driven particles at fluid interfaces acting as capillary dipoles. *J. Fluid Mech.* 770:5–26

Dolinsky Y, Elperin T. 2009. Electrorotation of a leaky dielectric spheroid immersed in a viscous fluid. *Phys. Rev. E* 80:066607

Dommersnes P, Rozynek Z, Mikkelsen A, Castberg R, Kjerstad K, et al. 2013. Active structuring of colloidal armor on liquid drops. *Nature Communications* 4:2066

Dubash N, Mestel AJ. 2007. Behaviour of a conducting drop in a highly viscous fluid subject to an electric field. *J. Fluid Mech.* 581:469–493

Esmaeeli A, Sharifi P. 2011. Transient electrohydrodynamics of a liquid drop. *Phys. Rev. E* 84:036308

Evans E, Rawicz W. 1990. Entropy driven tension and bending elasticity in condensed-fluid membranes. *Phys. Rev. Lett.* 64:2094–2097

Feng JQ. 1996. Dielectrophoresis of a deformable fluid particle in a non-uniform electric field. *Phys. Rev. E* 54:4438–441

Fernandez A. 2008a. Response of an emulsion of leaky dielectric drops immersed in a simple shear flow: Drops less conductive than the suspending fluid. *Phys. Fluids* 20:043304

Fernandez A. 2008b. Response of an emulsion of leaky dielectric drops immersed in a simple shear flow: Drops more conductive than the suspending fluid. *Phys. Fluids* 20:043303

Ganan-Calvo AM, Lopez-Herrera JM, Herrada MA, Ramos A, Montanero JM. 2018. Review on the physics of electrospray: From electrokinetics to the operating conditions of single and coaxial taylor cone-jets, and ac electrospray. *Journal of Aerosol Science* :in press

Ganan-Calvo AM, Lopez-Herrera JM, Rebollo-Munoz N, Montanero JM. 2016. The onset of electrospray: the universal scaling laws of the first ejection. *Scientific reports* 6:32357

Ghazian O, Adamiak K, Castle GSP, Higashiyama Y. 2014. Oscillation, pseudo-rotation and coalescence of sessile droplets in a rotating electric field. *Coll. Surf. A* 441:346–353

Grosse C, Schwan HP. 1992. Cellular membrane potentials induced by alternating fields. *Biophys. J.* 63:1632–1642

Ha JW, Yang SM. 1995. Effects of surfactant on the deformation and stability of a drop in a viscous fluid in an electric field. *J.Coll. Int. Sci.* 175:369–385

Ha JW, Yang SM. 1998. Effect of nonionic surfactant on the deformation and breakup of a drop in an electric field. *J. Coll. Int. Sci.* 206:195–204

Ha JW, Yang SM. 2000a. Electrohydrodynamics and electrorotation of a drop with fluid less conductive than that of the ambient fluid. *Phys. Fluids* 12:764–772

Ha JW, Yang SM. 2000b. Rheological responses of oil-in-oil emulsions in an electric field. *J. Rheol.* 44:235–256

Haluska C, Marchi-Artzner V, Brienne J, Lehn L, Lipowsky R, Dimova R. 2004. Fusion of giant vesicles observed with time resolution below millisecond. *Biophys. J.* 86:519A

He H, Salipante PF, Vlahovska PM. 2013. Electrorotation of a viscous droplet in a uniform direct current electric field. *Phys. Fluids* 25:032106

Hu Y, Miksis M, Vlahovska PM. 2018. Forces on a conducting spherical particle at a fluid interface. *SIAM J Appl. Math* submitted

Huang HF, Zahn M, Lemaire E. 2011. Negative electrorheological responses of micro-polar fluids in the finite spin viscosity small spin velocity limit. i. couette flow geometries. *J. Electrostatics* 69:442–455

Jones TB. 1984. Quincke rotation of spheres. *IEEE Trans. Industry Appl.* 20:845–849

Karyappa RB, Deshmukh SD, Thaokar RM. 2014. Breakup of a conducting drop in a uniform electric field. *J. Fluid Mech.* 754:550–589

Kim S, Karrila SJ. 1991. Microhydrodynamics: Principles and selected applications. Butterworth-Heinemann

Knorr RL, Staykova M, Gracia RS, Dimova R. 2010. Wrinkling and electroporation of giant vesicles in the gel phase. *Soft Matter* 6:1990–1996

Kokot G, Das S, Winkler RG, Gompper G, Aranson IS, Snezhko A. 2017. Active turbulence in a gas of self-assembled spinners. *PNAS* 114:12870–12875

Kolahdouz EM, Salac D. 2015a. Dynamics of three-dimensional vesicles in dc electric fields. *Phys. Rev. E* 92:012302

Kolahdouz EM, Salac D. 2015b. Electrohydrodynamics of three-dimensional vesicles: a numerical approach. *SIAM J. Sci. Comput.* 37:B473–B494

Lac E, Homsy GM. 2007. Axisymmetric deformation and stability of a viscous drop in a steady electric field. *J. Fluid. Mech* 590:239–264

Lacoste D, Lagomarsino M, Joanny J. 2007. Fluctuations of a driven membrane in an electrolyte. *Europhys. Lett.* 77:18006

Lacoste D, Menon GI, Bazant MZ, Joanny JF. 2009. Electrostatic and electrokinetic contributions to the elastic moduli of a driven membrane. *Eur. Phys. J. E* 28:243–264

Lanauze JA, Walker LM, Khair AS. 2013. The influence of inertia and charge relaxation on electrohydrodynamic drop deformation. *Phys. Fluids* 25:112101

Lanauze JA, Walker LM, Khair AS. 2015. Nonlinear electrohydrodynamics of slightly deformed oblate drops . *J. Fluid Mech,* 774:245–266

Larson RG. 1999. The structure and rheology of complex fluids. Oxford: Oxford University Press

Lavrentovich OD. 2016. Active colloids in liquid crystals. *Current Opinion in Colloid and Interface Sci.* 21:97–109

Lemaire E, Lobry L. 2002. Chaotic behavior in electro-rotation. *Physica A* 314:663–671

Lemaire E, Lobry L, Pannacci Na. 2008. Viscosity of an electro-rheological suspension with internal rotations. *J. Rheology* 52:769–783

Loubet B, Hansen PL, Lomholt MA. 2013. Electromechanics of a membrane with spatially distributed fixed charges: Flexoelectricity and elastic parameters. *Phys. Rev. E* 88:062715

Malkus WVR, Veronis G. 1961. Surface electroconvection. *Phys. Fluids* 4:13–23

Mandal S, Chakraborty S. 2017a. Effect of uniform electric field on the drop deformation in simple shear flow and emulsion shear rheology. *Phys. Fluids* 29:072109

Mandal S, Chakraborty S. 2017b. Influence of interfacial viscosity on the dielectrophoresis of drops. *Phys. Fluids* 29:052002

Mandal S, Chakraborty S. 2017c. Uniform electric-field-induced non-newtonian rheology of a dilute suspension of deformable newtonian drops. *Phys. Rev. Fluids* 2:093602

McConnell LC, Miksis MJ, Vlahovska PM. 2013. Vesicle electrohydrodynamics in dc electric fields. *IMA J. Appl. Math.* 78:797–817

McConnell LC, Miksis MJ, Vlahovska PM. 2015a. Continuum modeling of the electric-field-induced tension in deforming lipid vesicles. *J. Chem. Phys.* 143:243132

McConnell LC, Miksis MJ, Vlahovska PM. 2015b. Vesicle dynamics in uniform electric fields: squaring and breathing. *Soft Matter* 11:4840–4846

Melcher JR, Taylor GI. 1969. Electrohydrodynamics - a review of role of interfacial shear stress. *Annu. Rev. Fluid Mech.* 1:111–146

Mikkelsen A, Rozynek Z, Khobaib K, Dommersnes P, Fossum JO. 2017. Transient deformation dynamics of particle laden droplets in electric field. *Colloids and Surfaces A* 532:252–256. 30th Meeting of the European-Colloid-and-Interface-Society (ECIS), La Sapienza Univ Rome, Rome, ITALY, SEP 04-09, 2016

Mori Y, Young YN. 2018. Electrohydrodynamics of leaky dielectrics as the weak electrolyte limit of an electrodiffusion model. *arXiv:1709.02321*

Nganguia H, Young YN, Layton AT, Hu WF, Lai MC. 2015. An Immersed Interface Method for Axisymmetric Electrohydrodynamic Simulations in Stokes flow. *Comm. Comp. Phys.* 18:429–449

Nganguia H, Young YN, Vlahovska PM, Blawzdziewcz J, Zhang J, Lin H. 2013. Equilibrium electrodeformation of a surfactant-laden viscous drop. *Phys. Fluids* 25:092106

Ouriemi M, Vlahovska PM. 2014. Electrohydrodynamics of particle-covered drops. *J. Fluid Mech.* 751:106–120

Ouriemi M, Vlahovska PM. 2015. Electrohydrodynamic deformation and rotation of a particle-coated drop. *Langmuir* 31:6298–6305

Pairam E, Fernández-Nieves A. 2009. Generation and stability of toroidal droplets in a viscous liquid. *Phys. Rev. Lett.* 102:234501

Pan XD, McKinley GH. 1997. Characteristics of electrorheological responses in an emulsion system. *J. Coll. Int. Sci.* 195:101–113

Pascall AJ, Squires TM. 2011. Electrokinetics at liquid/liquid interfaces. *J. Fluid Mech.* 684:163–191

Perrier DL, Rems L, Boukany PE. 2017. Lipid vesicles in pulsed electric fields: Fundamental prin-

ciples of the membrane response and its biomedical applications. *Adv. Colloid Interface Sci.* 249:248–271

Pillai R, Berry JD, Harvie DJE, Davidson MR. 2016. Electrokinetics of isolated electrified drops. *Soft Matter* 12:3310–3325

Portet T, Dimova R. 2010. A new method for measuring edge tensions and stability of lipid bilayers: Effect of membrane composition. *Biophys. Journal* 99:3264–3273

Portet T, Mauroy C, Demery V, Houles T, Escoffre JM, et al. 2012. Destabilizing Giant Vesicles with Electric Fields: An Overview of Current Applications. *J. Membrane Biology* 245:555–564

Riske KA, Dimova R. 2005. Electro-deformation and poration of giant vesicles viewed with high temporal resolution. *Biophys. J.* 88:1143–1155

Riske KA, Dimova R. 2006. Electric pulses induce cylindrical deformations on giant vesicles in salt solutions. *Biophys. J.* 91:1778–1786

Riske KA, Knorr RL, Dimova R. 2009. Bursting of charged multicomponent vesicles subjected to electric pulses. *Soft Matter* 5:1983–1986

Rozynek Z, Castberg R, Kalicka A, Jankowski P, Garstecki P. 2015. Electric field manipulation of particles in leaky dielectric liquids. *Archives of Mechanics* 67:385–399

Rozynek Z, Mikkelsen A, Dommersnes P, Fossum JO. 2014. Electroformation of Janus and patchy capsules. *Nature Comm.* 5

Salipante PF, Knorr R, Dimova R, Vlahovska PM. 2012. Electrodeformation method for measuring the capacitance of bilayer membranes. *Soft Matter* 8:3810– 3816

Salipante PF, Shapiro ML, Vlahovska PM. 2015. Electric field induced deformations of biomimetic fluid membranes. *Procedia IUTAM* 16:60 – 69

Salipante PF, Vlahovska PM. 2010. Electrohydrodynamics of drops in strong uniform dc electric fields. *Phys. Fluids* 22:112110

Salipante PF, Vlahovska PM. 2013. Electrohydrodynamic rotations of a viscous droplet. *Phys. Rev. E* 88:043003

Salipante PF, Vlahovska PM. 2014. Vesicle deformation in dc electric pulses. *Soft Matter* 10:3386 –3393

Sato H, Kaji N, Mochizuki T, Mori YH. 2006. Behavior of oblately deformed droplets in an immiscible dielectric liquid under a steady and uniform electric field. *Phys. Fluids* 18:127101

Saville DA. 1997. Electrohydrodynamics: The Taylor-Melcher leaky dielectric model. *Annu. Rev.Fluid Mech.* 29:27–64

Schnitzer O, Frankel I, Yariv E. 2013a. Deformation of leaky-dielectric fluid globules under strong electric fields: boundary layers and jets at large Reynolds numbers. *J. Fluid Mech.* 734:R3

Schnitzer O, Frankel I, Yariv E. 2013b. Electrokinetic flows about conducting drops. *J. Fluid Mech.* 722:394–423

Schnitzer O, Yariv E. 2013. Nonlinear electrokinetic flow about a polarized conducting drop. *Phys. Rev E* 87:041002

Schwalbe J, Vlahovska PM, Miksis MJ. 2011a. Lipid membrane instability driven by capacitive charging. *Physics of Fluids* 23:041701

Schwalbe J, Vlahovska PM, Miksis MJ. 2011b. Vesicle electrohydrodynamics. *Phys. Rev E* 83:046309

Seifert U. 1997. Configurations of fluid membranes and vesicles. *Advances in physics* 46:13–137

Seifert U. 1999. Fluid membranes in hydrodynamic flow fields: Formalism and an application to fluctuating quasispherical vesicles. *Eur. Phys. J. B* 8:405–415

Seifert U, Langer S. 1993. Viscous modes of fluid bilayer membranes. *Europhys. Lett.* 23:71–76

Seiwert J, Miksis MJ, Vlahovska PM. 2012. Stability of biomimetic membranes in dc electric fields. *J. Fluid Mech.* 706:58–70

Seiwert J, Vlahovska PM. 2012. Instability of a fluctuating membrane driven by an ac electric field. *Phys. Rev. E* 87:022713

Sengupta R, Walker LM, Khair AS. 2017. The role of surface charge convection in the electrohydrodynamics and breakup of prolate drops. *J. Fluid Mech.* 833:29–53

Sens P, Isambert H. 2002. Undulation instability of lipid membranes under an electric field. *Phys. Rev. Lett.* 88:Art. No. 128102

Sheng P, Wen W. 2012. Electrorheological Fluids: Mechanisms, Dynamics, and Microfluidics Applications. In *ANNUAL REVIEW OF FLUID MECHANICS, VOL 44*, ed. Davis, SH and Moin, P, vol. 44 of *Annual Review of Fluid Mechanics*. 143+

Sinha KP, Gadkari S, Thaokar RM. 2013. Electric field induced pearling instability in cylindrical vesicles. *Soft Matter* 9:7274–7293

Snezhko A. 2016. Complex collective dynamics of active torque-driven colloids at interfaces. *Current Opinion Coloid and Interface Sci.* 21:65–75

Staykova M, Lipowsky R, Dimova R. 2008. Membrane flow patterns in multicomponent giant vesicles induced by alternating electric fields. *Soft Matter* 4:2168–2171

Suryo R, Basaran OA. 2006. Tip streaming from a liquid drop forming from a tube in a co-flowing outer fluid. *Phys. Fluids* 18

Tadavani SK, Munroe JR, Yethiraj A. 2016. The effect of confinement on the electrohydrodynamic behavior of droplets in a microfluidic oil-in-oil emulsion. *Soft Matter* 12:9246–9255

Taylor GI. 1932. The viscosity of a fluid containing small drops of another fluid. *Proc. R. Soc. A* 138:41

Taylor GI. 1966. Studies in electrohydrodynamics. I. Circulation produced in a drop by an electric field. *Proc. Royal Soc. A* 291:159–166

Torza S, Cox R, Mason S. 1971. Electrohydrodynamic deformation and burst of liquid drops. *Phil. Trans. Royal Soc. A* 269:295–319

Tseng YH, Prosperetti A. 2015. Local interfacial stability near a zero vorticity point. *J. Fluid Mech.* 776:5–36

Turcu I. 1987. Electric field induced rotation of spheres. *J. Phys. A: Math. Gen.* 20:3301–3307

Tyatyushkin AN. 2017. Unsteady electrorotation of a drop in a constant electric field. *Phys. Fluids* 29:097101

van Blaaderen A, Dijkstra M, van Roij R, Imhof A, Kamp M, et al. 2013. Manipulating the self assembly of colloids in electric fields. *Eur. Phys. J -Special Topics* 222:2895–2909

Varshney A, Gohil S, Sathe M, Yethiraj A. 2016. Multiscale flow in an electro-hydrodynamically driven oil-in-oil emulsion. *Soft Matter* 12:1759–1764

Veerapaneni S. 2016. Integral equation methods for vesicle electrohydrodynamics in three dimensions. *J. Comp. Physics* 326:278–289

Vlahovska P, Bławzdziewicz J, Loewenberg M. 2009a. Small-deformation theory for a surfactant-covered drop in linear flows. *J. Fluid Mech.* 624:293–337

Vlahovska PM. 2010. Non-equilibrium dynamics of lipid membranes: deformation and stability in electric fields. In *Advances in Planar Lipid Bilayers and Liposomes, vol. 12*, ed. A Iglic. Elsevier, 103–146

Vlahovska PM. 2015. Voltage-morphology coupling in biomimetic membranes: dynamics of giant vesicles in applied electric fields. *Soft Matter* 11:7232–7236

Vlahovska PM. 2016. Dynamics of membrane bound particles: capsules and vesicles. In *Low-Reynolds-Number Flows: Fluid-Structure Interactions*, eds. C Duprat, H Stone. Royal Society of Chemistry Series RSC Soft Matter

Vlahovska PM. 2016. Electrohydrodynamic instabilities of viscous drops. *Phys. Rev. Fluids* 1:060504

Vlahovska PM, Gracia RS, Aranda-Espinoza S, Dimova R. 2009b. Electrohydrodynamic model of vesicle deformation in alternating electric fields. *Biophys. J.* 96:4789–4803

Weaver JC, Chizmadzhev YA. 1996. Theory of electroporation: A review. *Bioelectrochem.Bioenerg.* 41:135–160

Wu B, Veerapaneni S. 2018. Pairwise hydrodynamic interactions of deflated vesicles in uniform electric fields. *J. Fluid Mech.* under review

Yamamoto T, Aranda-Espinoza S, Dimova R, Lipowsky R. 2010. Stability of spherical vesicles in electric fields. *Langmuir* 26:12390–12407

Yariv E, Frankel I. 2016. Electrohydrodynamic rotation of drops at large electric Reynolds numbers. *J. Fluid Mech.* 788:R2

Yariv E, Rhodes D. 2013. Electrohydrodynamic drop defamation by strong electric fields: slender body analysis. *SIAM J. Appl. Math.* 73:2143–2161

Yeo K, Lushi E, Vlahovska PM. 2015. Collective dynamics in a binary mixture of hydrodynamically coupled microrotors. *Phys. Rev. Lett.* 114:188301

Young YN, Miksis M. 2015. Electrohydrodynamics instability of a capacitive elastic membrane. *Phys. Fluids* 27:022102

Young YN, Veerapaneni S, Miksis M. 2014. Long-wave dynamics of an inextensible planar membrane in an electric field. *J. Fluid Mech.* 751:406–431

Yu M, Lira RB, Riske KA, Dimova R, Lin H. 2015. Ellipsoidal Relaxation of Deformed Vesicles. *Phys. Rev. Lett.* 115

Zabarankin M. 2013. A liquid spheroidal drop in a viscous incompressible fluid under a steady electric field. *SIAM J. Appl. Math.* 73:677–699

Zabarankin M, Smagin I, Lavrenteva OM, Nir A. 2013. Viscous drop in compressional Stokes flow. *J. Fluid. Mech.* 720:169–191

Zhang J, Song Y, Li D. 2018. Electrokinetic motion of a spherical polystyrene particle at a liquid-fluid interface. *J. Colloid Int. Sci.* 509:432–439

Zhang J, Zahn JD, Lin H. 2013a. Transient solution for droplet deformation under electric fields. *Phys. Rev. E* 87:043008

Zhang J, Zahn JD, Tan W, Lin H. 2013b. A transient solution for vesicle electrodeformation and relaxation. *Phys. Fluids* 25:071903

Zholkovskij EK, Masilyah JH, Czarnecki J. 2002. An electrokinetic model of drop deformation in an electric field. *J. Fluid Mech.* 472:1–27

Ziebert F, Bazant MZ, Lacoste D. 2010. Effective zero-thickness model for a conductive membrane driven by an electric field. *Phys. Rev. E* 81:031912

Ziebert F, Lacoste D. 2010. A poisson-boltzmann approach for a lipid membrane in an electric field. *New J. Phys.* 12:095002

Ziebert F, Lacoste D. 2011. A planar lipid bilayer in an electric field: membrane instability, flow field and electrical impedance. In *Advances in Planar Lipid Bilayers and Liposomes, vol. 14*, ed. A Iglic. Elsevier, 63–95